Brain Tumor Characterization Using Multibiometric Evaluation of MRI

Faris Durmo[1], Jimmy Lätt[2], Anna Rydelius[3], Silke Engelholm[4], Sara Kinhult[4], Krister Askaner[2,5], Elisabet Englund[6], Johan Bengzon[7], Markus Nilsson[1], Isabella M. Björkman-Burtscher[1,2,8], Thomas Chenevert[9], Linda Knutsson[10,11], and Pia C. Sundgren[1,2,9]

[1]Department of Radiology, Clinical Sciences Lund, Lund University, Lund, Sweden; [2]Centre for Medical Imaging and Physiology, Skåne University Hospital, Lund and Malmö, Sweden; [3]Department of Neurology, Clinical Sciences Lund, Lund University, Lund, Sweden; [4]Department of Oncology, Clinical Sciences Lund, Lund University, Lund, Sweden; [5]Department of Radiology, Translational Medicine, Lund University, Lund, Sweden; [6]Department of Pathology, Clinical Sciences Lund, Lund University, Lund, Sweden; [7]Department of Neurosurgery, Clinical Sciences Lund, Lund University, Lund, Sweden; [8]Lund University Biolmaging Centre (LBIC), Lund University, Lund, Sweden; [9]Department of Radiology, University of Michigan, Ann Arbor, MI; [10]Department of Medical Radiation Physics, Clinical Sciences Lund, Lund University, Lund, Sweden; and [11]Department of Radiology and Radiological Science, Johns Hopkins University, Baltimore, MD

Corresponding Author:
Faris Durmo, Bmed
Department of Radiology, Clinical Sciences Lund, Lund University,
221 85 Lund, Sweden;
E-mail: lak14fdu@student.lu.se

ABSTRACT

The aim was to evaluate volume, diffusion, and perfusion metrics for better presurgical differentiation between high-grade gliomas (HGG), low-grade gliomas (LGG), and metastases (MET). For this retrospective study, 43 patients with histologically verified intracranial HGG (n = 18), LGG (n = 10), and MET (n = 15) were chosen. Preoperative magnetic resonance data included pre- and post-gadolinium contrast-enhanced T1-weighted fluid-attenuated inversion recover, cerebral blood flow (CBF), cerebral blood volume (CBV), fractional anisotropy, and apparent diffusion coefficient maps used for quantification of magnetic resonance biometrics by manual delineation of regions of interest. A binary logistic regression model was applied for multiparametric analysis and receiver operating characteristic (ROC) analysis. Statistically significant differences were found for normalized-ADC-tumor (nADC-T), normalized-CBF-tumor (nCBF-T), normalized-CBV-tumor (nCBV-T), and normalized-CBF-edema (nCBF-E) between LGG and HGG, and when these metrics were combined, HGG could be distinguished from LGG with a sensitivity and specificity of 100%. The only metric to distinguish HGG from MET was the normalized-ADC-E with a sensitivity of 68.8% and a specificity of 80%. LGG can be distinguished from MET by combining edema volume (Vol-E), Vol-E/tumor volume (Vol-T), nADC-T, nCBF-T, nCBV-T, and nADC-E with a sensitivity of 93.3% and a specificity of 100%. The present study confirms the usability of a multibiometric approach including volume, perfusion, and diffusion metrics in differentially diagnosing brain tumors in preoperative patients and adds to the growing body of evidence in the clinical field in need of validation and standardization.

INTRODUCTION

Glioblastomas are the most common malignant neoplasms of the brain and together with metastatic tumors comprise half of all the malignant tumors of the brain (1). The recent published 2016 World Health Organization (WHO) classification of the central nervous system tumors incorporates, for the first time, molecular parameters in addition to histology to define brain tumors (2). The 2016 WHO central nervous system tumor classification divides glioblastoma tumors into (1) glioblastoma isocitrate dehydrogenase (IDH)-wild type (90% of cases, pre-

senting de novo in elderly patients), (2) glioblastoma IDH–mutant (10% of cases, the so-called secondary glioblastoma as the tumor often progresses from a low–grade tumor, predominately seen in younger patients), and (3) glioblastoma not–otherwise-specified tumor, in which complete IDH evaluation and histopathology cannot be performed or is inconclusive (2). The risk to develop a glioma of a certain grade increases with certain mutations (3).

Grading presumes biological behavior or phenotype of a lesion and is, together with molecular testing, of high clinical

importance for therapy selection; adjuvant radiation, chemo-therapy, surgical or palliative treatment. Gliomas of different grades may at presentation or over time exhibit morphological similarities on magnetic resonance imaging (MRI) (3).

In the present study, full molecular testing of the tumors was not performed in the majority of the patients. Therefore, they are referred to as high-grade gliomas (HGGs), that is, grades III–IV glioblastoma or low-grade gliomas (LGGs) according to the WHO classification 2016, with no reference to different mutations (2). MRI is considered the standard modality for diagnosis and prognosis of brain tumors, based primarily on gadolinium (Gd) contrast medium enhancement, biological behavior including location, and progression over time. This concept, however, is challenging, as not all HGGs show Gd enhancement. Further, 10% of glioblastomas and 30% of anaplastic astrocytomas do not enhance, whereas few LGGs occasionally do enhance (4). Clinical distinction between LGG and HGG is important, as the treatment options between these groups may significantly differ. The clinically estimated prognosis for each patient with a certain type of tumor includes prognostic factors such as age of patient, tumor location, contrast enhancement, and residual postoperative tumor volume (5–9). The largest tumor diameter has an impact on survival for patients with LGG, and extensive surgical resection is beneficial (10). However, HGGs are today treated more aggressively than LGGs, as the overall survival (OS) for patients with LGG is substantially longer than that for patients with HGG (2). Intracranial metastases (MET) may have a similar imaging appearance, as solid or ring-enhancing cystic lesions may, in the initial stage, complicate the differentiation toward HGG (11). Different MRI techniques such as perfusion-weighted MRI, diffusion-weighted imaging (DWI), and diffusion tensor imaging have a diagnostic value for the discrimination between LGG and HGG and for identifying the glioma grade (12, 13).

In this study, it is proposed that LGG/HGG/MET have sufficiently different manifestations at early presentation of the disease, allowing for clinically acceptable discrimination by utilization of several MRI protocols. Aggressive growth in HGG is hypothesized to manifest with a higher tumor volume (Vol-T), normalized cerebral blood flow (nCBF-T), normalized cerebral blood volume-tumor (nCBV-T), normalized fractional anisotropy-tumor (nFA-T), normalized fractional anisotropy-edema (nFA-E), nCBF-edema (nCBF-E), and nCBV-edema (nCBV-E), and a lower nADC-T, nADC-E, ratio edema volume to tumor volume (Vol-E/Vol-T), compared with LGG and MET. It is hypothesized that the differences between MET and HGG, both presenting as highly malignant and proliferating entities, are distinguishable, albeit having smaller differences than when comparing LGG and HGG owing to LGG's generally low proliferating state. It is hypothesized that aggressive growth is associated with higher vascularity, cellular density, and destruction of the myelin, which, in turn, is quantifiable by measuring diffusion, perfusion, and volumes of tumor and edema. Aggressive growth as seen in HGG, is hypothesized to manifest with higher intratumoral and peritumoral perfusion, greater tumor volume, and lower diffusion when compared with MET and LGG. The low proliferative state of LGG and the probable vasogenic edema around MET are hypothesized to result in lower perfusion values and higher diffusion values in edematous tissue than in edematous tissue of

HGGs, which probably has a more infiltrative component than LGG and MET.

Utilization of the microstructure either within the tumor or adjacent to the tumor, that is, perilesional tissue, has been reported with varying degrees of success in differential diagnosis between MET and HGG (13). Tumoral and peritumoral CBV, ADC, and FA provide diagnostic information in the differentiation between LGG and HGG (13). In addition, there is potential in measuring the ratio between Vol-E and Vol-T for the differentiation between MET and what was formerly categorized by WHO as glioblastoma multiforme (14). However, conflicting evidence exists, in which imaging biomarkers are optimal and should be used for the distinction between HGG, LGG, and MET (12, 15). A similar morphological appearance on MRI, along with varying treatment options and varying overall prognoses, raises the necessity for standardized and verified protocols to increase the specificity of MRI regarding the differentiation of HGG, LGG, and MET.

Because the further treatment approach is reflected by the suspected diagnosis, the possibility to separate these entities may reduce the need for surgery and histopathology confirmation, particularly between LGG and MET and HGG and MET. Ultimately, this study, when externally validated, may help to establish a minimally invasive approach to earlier screening for disease, more rapid diagnosis of patients, and decision support for clinicians (16).

The aim of this study is to evaluate the sensitivity and specificity of advanced magnetic resonance (MR) imaging metrics for DWI, perfusion-weighted MRI and tumor and edema volume for tumor type differentiation in a cohort of patients with HGG, LGG, and MET.

MATERIALS AND METHODS

The initial cohort of this retrospective study consisted of 60 consecutive patients. After excluding patients with meningioma, lesions at the skull base, and those that had limited preoperative MR examination, the final cohort consisted of 43 patients; 18 HGG (15 glioblastomas, grade IV; 2 oligoastrocytomas, grade III; 1 anaplastic oligoastrocytoma, grade III), 10 LGG (3 diffuse astrocytomas, grade II; 4 astrocytomas, grade II; 2 oligodendrogliomas, grade II; and 1 oligoastrocytoma, grade II), and 15 MET (9 adenocarcinomas with gastrointestinal, lung, or breast origin; 4 malignant melanomas; 1 invasive lobular breast carcinoma; and 1 anaplastic thyroid cancer). There were 30 male patients and 13 female patients with a mean age at diagnosis of 64 (range, 48–79) years for HGG, 45 (range, 20–66) years for LGG, and 59 (range, 30–81) years for MET. Study inclusion criteria were age >18 years, histologically verified intracranial glial tumor of de novo origin or brain MET and MRI performed before surgery. The study has been approved by the local ethical committee, and written informed consent was obtained from all study subjects (#2010/199, 2012/188, 2014/368).

Clinical Data

Histological diagnosis of tumors was obtained surgically by resection (n = 12 HGG, 6 LGG, 15 MET) or biopsy (n = 6 HGG, 4 LGG) (Table 1). Mean time to progression (MTP) (measured in days after initial MR imaging, on the basis of which the tumor was detected) and mean OS (measured in months after the

Table 1. Demographics, Tumor Type, Histopathology, Tumor Location, Type of Surgery, MTP, and OS

Patient/Sex/Age/Tumor Type	Histopathology (grade)	Location of Tumor	Type of Surgery	MTP	OS
1/F/54/HGG	GB (IV)	Frontal RT	Resection	106	9
2/M/48/HGG	OA (III)	Temporal LT	Resection	294	17
3/M/66/HGG	GB (IV)	Frontal RT	Resection	155	26
4/M/63/HGG	GB (IV)	Frontal RT	Resection	222	17
5/M/62/HGG	OA (III)	Frontal RT	Resection	480	19
6/M/60/HGG	GB (IV)	Temporal LT	Resection	>80	>3
7/F/68/HGG	GB (IV)	Frontal LT	Resection	233	>8
8/M/74/HGG	GB (IV)	Parietal LT	Needle biopsy	97	10
9/F/60/HGG	GB (IV)	Parietooccipital RT	Resection	292	28
10/F/59/HGG	GB (IV)	Temporooccipital LT	Resection	30	>7
11/M/66/HGG	GB (IV)	Temporal LT	Open biopsy	9	2
12/M/79/HGG	GB (IV)	Frontal LT	Open biopsy	146	6
13/M/60/HGG	GB (IV)	Parietotemporal RT	Open biopsy	*	>30
14/M/77/HGG	GB (IV)	Temporooccipital LT	Needle biopsy	99	>7
15/M/71/HGG	GB (IV)	Frontal LT	Extirpation	85	>14
16/M/60/HGG	Anaplastic OA (III)	Parietal LT	Open biopsy	139	15
17/M/65/HGG	GB (IV)	Temporal LT	Extirpation	30	29
18/M/56/HGG	GB (IV)	Parietal RT	Resection	280	>18
19/F/34/LGG	OA (II)	Frontal LT	Resection	>1099	>46
20/M/27/LGG	Astrocytoma (II)	Frontal RT	Extirpation	>935	>56
21/F/20/LGG	Oligodendroglioma (II)	Frontotemporal LT	Extirpation	>141	>55
22/M/56/LGG	Astrocytoma (II)	Temporal LT	Open biopsy	354	31
23/M/66/LGG	Diffuse astrocytoma (II)	Parietooccipital LT	Needle biopsy	281	12
24/M/51/LGG	Diffuse astrocytoma (II)	Temporal LT	Extirpation	184	>46
25/M/26/LGG	Oligodendroglioma (II)	Parietal RT	Resection	>17	>1
26/M/52/LGG	Astrocytoma (II)	Temporal LT	Needle biopsy	28	>18
27/M/66/LGG	Diffuse astrocytoma (II)	Temporoparietal LT	Open biopsy	>15	>3
28/M/49/LGG	Oligodendroglioma (II)	Frontal RT	Resection	*	>26
29/F/81/MET	AC lung	Cerebellum RT	Extirpation	*	>71
30/M/75/MET	Melanoma	Frontotemporal LT	Extirpation	*	3
31/M/59/MET	AC gastrointestinal	Parietal RT	Extirpation	*	6
32/M/47/MET	AC colorectal	Occipital LT	Extirpation	*	16
33/M/77/MET	Melanoma	Frontal LT	Resection	*	7
34/F/54/MET	Invasive lobular carcinoma lung	Cerebellum RT	Resection	*	>2
35/M/49/MET	AC lung	Cerebellum LT	Extirpation	*	8
36/M/45/MET	Melanoma	Parietal LT	Extirpation	*	7
37/F/73/MET	AC breast	Cerebellum LT	Extirpation	*	17
38/M/59/MET	Melanoma	Frontal RT	Extirpation	*	9
39/F/73/MET	AC lung	Cerebellum RT	Extirpation	*	>51
40/F/56/MET	AC lung	Temporal LT	Extirpation	*	6
41/F/30/MET	AC breast	Parietal LT	Extirpation	*	38
42/F/53/MET	AC colorectal	Frontal LT	Extirpation	*	>1
43/M/54/MET	anaplastic thyroid cancer	Frontal LT	Extirpation	*	3

Abbreviations: GB, glioblastoma; OA, oligoastrocytoma; MET, metastasis; AC, adenocarcinoma; LT, left; RT, right.
* Data not obtainable; resection refers to partial resection of the tumor; extirpation refers to total resection of the tumor.

aforementioned initial MRI examination until death or last available follow-up) were calculated for each group (Table 1) and derived from patients' medical records based on the combination of clinical evaluation and radiological findings. For the radiological decision, the RANO (Response Assessment in Neuro-Oncology) criteria were used.

Study Protocol

MRI was performed on a 3 T Siemens MAGNETOM Skyra® (Erlangen, Germany), with a 20-channel head/neck coil. The MR protocol included the following sequences: axial T2 2D Turbo spin-echo (TSE); axial 2D fluid attenuated inversion recovery (FLAIR); T1 3D magnetization prepared rapid gradient echo (MPRAGE), pre- and post-Gd contrast administration with 1-mm isotropic resolution; DWI; diffusion tensor imaging with diffusion-sensitized single-shot echo planar imaging (SSEPI) using 30 noncollinear diffusion gradient directions, with b-values of 0 and 1000 s/mm^2, and a spatial resolution of 2.0 × 2.0 × 2.0 mm^3; dynamic susceptibility contrast perfusion MR with a time resolution of 1.5 seconds, using a single-shot gradient echo EPI-gradient sequence, with a spatial resolution of 1.7 × 1.7 × 5.0 mm^3 and an echo time of 28 milliseconds. The total examination time was approximately 1 hour.

Postprocessing

All data were anonymized before any processing or export, according to local policies and stated in the ethical permission and written informed consent form. ADC and FA maps were calculated using in-house–developed software, based on the MATLAB framework. T1-weighted and FLAIR maps used for volume measurements were also calculated using the in-house–developed software, whereas the resulting perfusion maps were calculated using singular value decomposition with a truncated singular value decomposition and the software package Nordic ICE (NordicNeuroLab, Bergen, Norway; http://www.nordicneurolab.com/). All obtained perfusion maps were leakage-corrected with Boxerman and gamma fitting (Nordic ICE; NordicNeuroLab).

Biometrics

Tumor tissue was defined as a deranged tissue structure with or without Gd-enhancement, mass effect, hemorrhage, or necrosis but not solemnly attributed to perilesional edema. Biometrics included volume (Vol), nADC, nFA, nCBV, and nCBF for tumor and edema (Figure 1, A–N).

Manual region of interest (ROI) delineation has an advantage over semiautomatic segmentation for measurements on T2-weighted image maps, whereas semiquantitative methods of measurement underappreciate tumor volumes, suggesting that the manual approach is the method of choice for volumetric measurements on maps of T1-weighted image as well as T2-weigthed image (17). In addition, manual ROI delineation is a clinically acceptable method for the measurement of nCBV. Elliptic ROIs of a similar size and shape were chosen to reduce the risk of underappreciating the true value of the intended measurement. Also, the elliptical ROI was chosen to include more volume/area/tissue when measuring and to reduce the risk of encompassing tissues that do not require measurement, that is, not choosing a square ROI. The ROI location for normaliza-
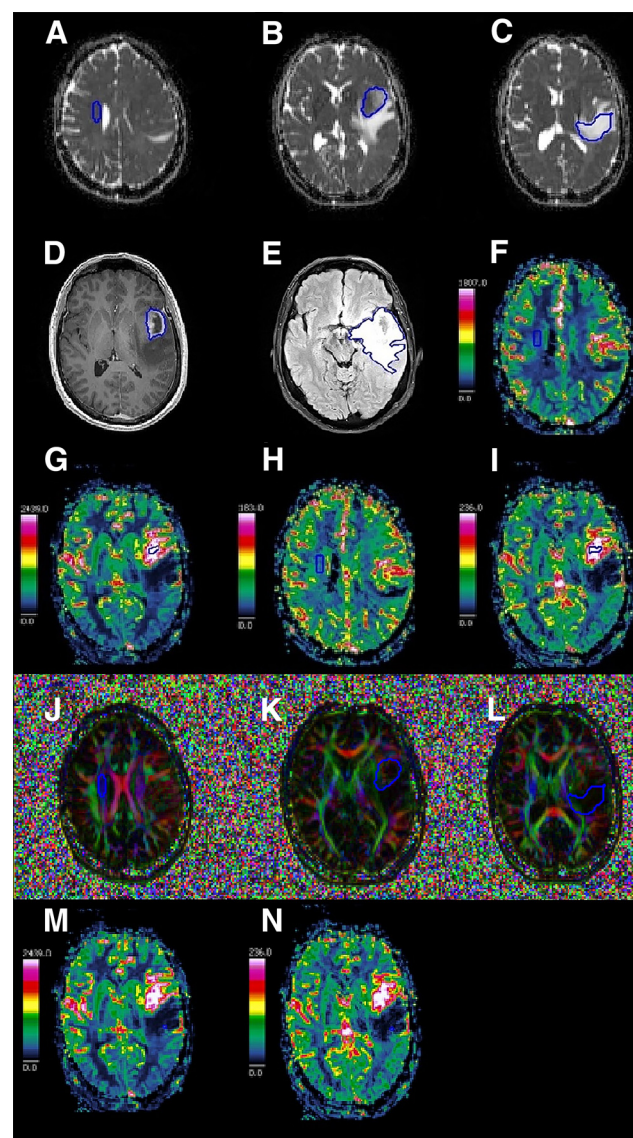

Figure 1. Illustration of manual delineation for quantification of apparent diffusion coefficient-normal appearing white matter (ADC-NAWM) (A), ADC-tumor (ADC-T) (B), ADC-edema (ADC-E) (C), tumor volume (Vol-T) (D), edema volume (Vol-E) (E), cerebral blood flow-NAWM (CBF-NAWM) (F), CBF-tumor (CBF-T) (G), cerebral blood volume-NAWM (CBV-NAWM) (H), CBV-tumor (CBV-T) (I), fractional anisotropy-NAWM (FA-NAWM) (J), FA-tumor (FA-T) (K), FA-edema (FA-E) (L), CBF-edema (CBF-E) (M), and CBV-edema (CBV-E) (N).

tion was consistent for all modalities, that is, centrum semiovale, contralateral to the tumor. The in-house–developed program chosen for the measurements produced a mean of the measured entity and also provided a histogram of the values within the measurements; care was taken to produce measurements with a normal distribution on histograms. In our cohort,

Table 2. Median Values With Range and Minimum and Maximum Values for Evaluated Biometrics for HGG, LGG, and MET

Groups	Vol-T (mL)	Vol-E (mL)	Vol-E/Vol-T	nFA-T	nADC-T	nFA-E	nADC-E	nCBF-T	nCBV-T	nCBF-E	nCBV-E
HGG											
N	18	17	17	16	16	16	16	15	15	14	14
Median	40.25	26.58	0.83	0.40	1.52	0.47	1.49	7.91	6.65	0.59	0.68
Range	93.40	155.79	9.40	0.41	0.93	0.33	1.49	9.63	5.75	0.93	1.01
Minimum	1.57	0.46	0.01	0.15	1.16	0.23	1.13	2.55	2.70	0.40	0.34
Maximum	94.96	156.25	9.41	0.56	2.09	0.56	2.63	12.18	8.45	1.33	1.35
LGG											
N	10	10	10	10	10	10	10	10	10	10	10
Median	22.46	10.15	0.37	0.25	1.86	0.44	1.46	2.80	3.33	1.08	0.94
Range	59.50	38.07	0.85	0.16	0.85	0.24	0.56	2.33	4.97	1.34	1.19
Minimum	7.64	3.06	0.16	0.19	1.67	0.32	1.39	1.47	1.26	0.52	0.54
Maximum	67.14	41.13	1.01	0.35	2.52	0.56	1.96	3.79	6.22	1.86	1.74
MET											
N	15	15	15	15	15	15	15	15	15	15	15
Median	14.61	50.28	2.88	0.31	1.54	0.41	1.85	7.70	6.91	0.73	0.86
Range	66.04	109.39	6.51	0.31	1.14	0.24	1.29	8.17	9.29	1.12	1.95
Minimum	5.54	2.20	0.33	0.18	1.14	0.27	1.39	2.49	3.55	0.41	0.31
Maximum	71.57	111.58	6.84	0.49	2.28	0.51	2.68	10.67	12.84	1.53	2.25
Total											
N	43	42	42	41	41	41	41	40	40	39	39
Median	16.36	26.39	0.91	0.31	1.60	0.43	1.60	6.67	6.25	0.83	0.78
Range	93.40	155.79	9.40	0.41	1.38	0.33	1.55	10.71	11.58	1.47	1.95
Minimum	1.57	0.46	0.01	0.15	1.14	0.23	1.13	1.47	1.26	0.40	0.31
Maximum	94.96	156.25	9.41	0.56	2.52	0.56	2.68	12.18	12.84	1.86	2.25

Abbreviations: HGG, high-grade gliomas; LGG, low-grade gliomas; MET, metastases; nFA-T, normalized fractional anisotropy-tumor; nADC-T, normalized-ADC-tumor; nFA-E, normalized fractional anisotropy-edema; nADC-E, normalized-ADC-edema; nCBF-T, normalized cerebral blood flow-tumor; nCBV-T, normalized cerebral blood volume-tumor; nCBF-E, nCBF-edema; nCBV-E, nCBV-edema.

rectangular ROIs of size between 15 and 20 pixels produced poorer histograms than elliptical ROIs, probably owing to the inclusion of tissue that did not require measurement, that is, a rectangular-shaped ROI of size ≥15 pixels was not optimal for measurement. For CBF in edema, a rectangular-shaped ROI of size 4 pixels was chosen. The reduced-size ROI was used because of the hypothesis that the edematous tissue could be more prone to the partial volume effect. Regardless of the ROI size, the sampled value was averaged automatically by the program in which the measurements were made. Obtaining significant values across different modalities was an insurance of the stability of the measurements, as it showed that the method was reproducible. Therefore, an averaged measurement with a pixel size between 4 and 20 is sufficient for measurement.

Volume Metrics. For lesion volume (Vol-L), the outer margin of the entire lesion including tumor and edema was outlined on each section on the FLAIR maps, also referencing to T1- and T2-weighted maps. Total Vol-T was outlined in each section on the Gd-enhanced T1-weighted maps, also referencing to FLAIR and T2-weighted maps. Total edema volume (Vol-E) was calculated by subtraction of Vol-T, measured on the postcontrast T1-weighted images, from Vol-L; the entire Vol-L was measured on the FLAIR images for respective patients. Vol-E/Vol-T was calculated for all tumors. A neuroradiologist with 20 years of experience reassessed the volume delineation derived by a trainee MD and a PhD student.

Diffusion Metrics. Mean ADC and mean FA were measured for tumor and edema tissue (ADC-T, ADC-E, FA-T, and FA-E) in each patient. ROIs were defined on ADC and FA maps with reference to morphological images, avoiding necrotic, cystic, and hemorrhagic areas. For normalized values of ADC and FA, 1 ellipsoid ROI was placed on each of 3–4 sections (105–408 pixels in total for 3–4 ROIs per patient) in the normal-appearing white matter (NAWM) in the contralateral hemisphere using the centrum semiovale, more precisely craniocaudally oriented corona radiata fibers, for obtaining both nADC and nFA to obtain substantial representative tissue for mean FA-NAWM and mean ADC-NAWM values. This assumption for the normalization is supported by previous studies showing that normalized ADC values are more standardized than non-normalized values (15) and that ADC and FA values may be affected by age of the patients and tumor location in the brain (18). Normalized diffusion metrics were defined accordingly as nADC = ADC/ADC-NAWM and nFA = FA/FA-NAWM.

Table 3. Kruskal–Wallis *H* Test Between HGG, LGG, and MET

	Vol-T (mL)	Vol-E (mL)	Vol-E/Vol-T	nFA-T	nADC-T	nFA-E	nADC-E	nCBF-T	nCBV-T	nCBF-E	nCBV-E
Chi-square	2.562	7.337	10.522	4.760	12.876	2.656	8.928	18.211	13.453	7.791	4.619
P-value <	0.278	0.026	0.005	0.093	0.002	0.265	0.012	0.001	0.001	0.020	0.099

Abbreviations: HGG, high-grade gliomas; LGG, low-grade gliomas; MET, metastases; nFA-T, normalized fractional anisotropy-tumor; nADC-T, normalized-ADC-tumor; nFA-E, normalized fractional anisotropy-edema; nADC-E, normalized-ADC-edema; nCBF-T, normalized cerebral blood flow-tumor; nCBV-T, normalized cerebral blood volume-tumor; nCBF-E, nCBF-edema; nCBV-E, nCBV-edema.
Significance set at *P*-value <.05.

Perfusion Metrics. Areas with highest CBF and CBV values in tumor and edema areas were obtained by analysis of color-coded blood flow and volume maps as previously described (19). As suggested and used previously (20–22), four ellipsoid ROIs, each of size 18-20 pixels, were placed in areas of highest perfusion for each patient with reference to morphological images while avoiding necrotic, cystic, and hemorrhagic areas for maximum CBF-T and CBV-T values. The ellipsoid ROI with the highest CBF-T and CBV-T was then chosen to represent the maximum value; the other 3 ROIs were discarded. The maximum CBV-E and CBF-E values were obtained by means of an identical methodology with the exception of using a smaller rectangular ROI in edematous tissue versus tumor, that is, 1 rectangular ROI of 4 pixels on 1 section per patient.

The maximum CBV-T and CBV-E and CBF-T and CBF-E values were normalized to normal-appearing contralateral white matter using 1 rectangular ROI (38–40 pixels) placed in the contralateral hemisphere in the normal-appearing periventricular white matter in 1 section and by dividing tumor and edema values for each biometric by corresponding values of normal-appearing contralateral white matter, for example, nCBV-T = CBV-T/CBV-NAWM, as previously described (20). Because the present perfusion method does not allow for absolute values of CBV and CBF, the relative CBV and CBF value was calculated according to the standard method (23).

Statistical Analysis
Statistical analysis was performed with SPSS® v. 23.0 (IBM Corp., New York, NY; formerly SPSS Inc., Chicago, IL). A normality plot with a Shapiro–Wilk test was performed and Kruskal–Wallis *H* was chosen for comparison by rank medians between the 3 groups, namely, HGG, LGG, and MET. Kruskal–Wallis *H* was repeated for pairwise comparison between groups for those biometrics, which yielded a statistically nonsignificant difference with the initial Kruskal–Wallis *H* test. ε-Square estimation of the effect size was calculated for statistical significant results found by the Kruskal–Wallis

H test and Bonferroni adjustment was added before post hoc testing (24). Mann–Whitney *U* test was used for pairwise comparison between the groups and biometrics found to have statistically significant differences with Kruskal–Wallis *H* test. A binary logistic regression model was then used and an ROC analysis and univariate and multivariate analyses were performed with sensitivity and specificity calculated for each significant biometric. A multiple logistic regression analysis was performed and the probabilities were used in the ROC analysis.

Area under the curve (AUC), specificity, and sensitivity were used as indicators of performance for each ROC analysis (25). Finally, a Kaplan–Meier survival analysis was performed between the 3 groups. Statistical significance was set to *P*-value <.05.

RESULTS
Table 1 shows the demographics of the 43 patients included in this study. Of the 43 included, 4 patients with HGG were not evaluated for all biometrics because of the following technical issues: data were nonobtainable because of not performed or technical issues with selected sequences (FLAIR, nADC, nFA, nCBF, and nCBV) on the initial preoperative MRI examination (3 subjects) and extensive hemorrhagic volume in peritumoral edematous tissue for nCBF-E and nCBV-E (1 subject).

Mean Time to Progression and Overall Mean Survival
MTP for patients with HGG was 172 days (n = 15), and for patients with LGG was 211 days (n = 4). The Kaplan–Meier survival analysis showed that there were significant differences between the 3 groups with regard to OS; log rank, Breslow, Tarone–Ware *P*-value <.14; 0.01 and .01, respectively. OS for HGG (n = 18; 95% CI = 14–23) was 18.7 months, for LGG (n = 10; 95% CI = 34–57) was 46.2 months, and for MET (n = 15; 95% CI = 7-32) was 20.1 months (Table 1). Differences in MTP

Table 4. Comparison Between HGG and LGG Using Mann–Whitney *U* Test for HGG and LGG on Statistically Significant Biometrics

	Vol-E (mL)	Vol-E/Vol-T	nADC-T	nADC-E	nCBF-T	nCBV-T	nCBF-E	nCBV-E
Mann–Whitney *U*	44.00	55.00	22.00	71.00	7.00	14.00	25.00	33.00
P-value <	0.040	0.132	0.002	0.635	0.001	0.001	0.008	0.030

Abbreviations: HGG, high-grade gliomas; LGG, low-grade gliomas; MET, metastases; nADC-T, normalized-ADC-tumor; nADC-E, normalized-ADC-edema; nCBF-T, normalized cerebral blood flow-tumor; nCBV-T, normalized cerebral blood volume-tumor; nCBF-E, nCBF-edema; nCBV-E, nCBV-edema.
Significance after Bonferroni adjustment set at *P*-value <.016.

Table 5. Comparison Between HGG and MET Using Mann–Whitney *U* Test for HGG and MET on Previous Statistical Significant Biometrics

	Vol-E (mL)	Vol-E/Vol T	nADC-T	nADC-E	nCBF-T	nCBV-T	nCBF-E
Mann–Whitney *U*	103.00	85.00	116.00	58.00	92.00	100.00	97.00
P-value <	0.355	0.109	0.874	0.014	0.395	0.604	0.727

Abbreviations: HGG, high-grade gliomas; LGG, low-grade gliomas; MET, metastases; nADC-T, normalized-ADC-tumor; nADC-E, normalized-ADC-edema; nCBF-T, normalized cerebral blood flow-tumor; nCBV-T, normalized cerebral blood volume-tumor; nCBF-E, nCBF-edema.
Significance after Bonferroni adjustment set at *P*-value <.016.

between HGG and LGG could not be statistically evaluated owing to the sample consisting of fewer patients with LGG (n = 4).

Biometrics

Median, minimum, and maximum values for the evaluated biometrics are given for the 3 groups of HGG, LGG, and MET in Table 2. The Kruskal–Wallis *H* testing showed no significant differences between HGG, LGG, and MET for the following variables: Vol-T, nFA-T, and nFA-E and nCBV-E (Table 3). Pairwise analysis with Kruskal–Wallis *H*, after adjustment according to Bonferroni, confirmed no significant differences between the groups for these biometrics (*P*-value >.05), and these metrics were consequently excluded from the *a priori* post hoc testing. The effect size for the 3 groups and Vol-E, Vol-E/Vol-T, nADC-T, nADC-E, nCBF-T, nCBV-T, and nCBF-E was found to be E_{R^2} = 0.18, E_{R^2} = 0.26, E_{R^2} = 0.31, ER^2 = 0.22, ER^2 = 0.47, ER^2 = 0.34, ER^2 = 0.21, respectively. The variability in rank scores, accounted by group, was found to be the highest for nCBF-T with 47%.

Post Hoc Analysis

Bonferroni adjustment with a corrected alpha was performed and a conservative significance level of *P*-value <.016 (~0.0166) was chosen for post hoc testing. nADC-T, nCBF-T, nCBV-T, and nCBF-E in HGG differed significantly compared with LGG (Table 4). Further, nADC-E in HGG was significantly lower than that in MET (1.49 vs 1.85, respectively, *P* < .014) (Tables 2 and 5).

Vol-E, Vol-E/Vol-T, nADC-T, nADC-E, nCBF-T, and nCBV-T in LGG differed significantly compared with those in MET (Table 6). For specific values, see Table 2.

Binary Logistic Regression Model

The binary logistic regression model for HGG and LGG showed a *P*-value of <.001 for the model in the Omnibus tests and a Nagelkerke R^2 = 1.00, as well as *P*-values of <.003, <.001,

<.007, and <.002 for ADC-T, nCBF-T, nCBF-E, and nCBV-T, respectively. For LGG and MET, the binary logistic model showed a *P*-value of <0.001 for the model in the Omnibus tests and a Nagelkerke R^2 = 0.87, as well as *P*-values of <.010, <.003, <.003, <.007, <.001, and <.003 for Vol-E, Vol-E/Vol-T, nADC-T, nADC-E, nCBF-T, and nCBV-T, respectively. Statistical significant *P*-values and high Nagelkerke R^2 values disclosed that the model was adequate for the prediction of tumor type, which was also strengthened by the fact that 100% of the variance in the outcome was predicted for LGG and HGG by the statistically significant predictors, namely, nADC-T, nCBF-T, nCBF-E, and nCBV-T. In addition, Vol-E, Vol-E/Vol-T, nADC-T, nADC-E, nCBF-T, and nCBV-T succeeded in predicting 87% of the variance in tumor type between LGG and MET.

Receiver Operating Characteristic Analysis—Sensitivity and Specificity

Results of the ROC analysis are shown in Table 7. Univariate analysis with significant biometrics nADC-T, nCBF-T, nCBV-T, and nCBF-E for differentiation between HGG and LGG showed significant predictive ability for all 4 biometrics. However, nCBF-T (AUC = 0.95; *P*-value <.001) had the highest predictive capacity with a cutoff value of 4.12, sensitivity of 93.3%, and specificity of 100% (Figure 2, A and B; Table 7).

Differentiation between HGG and MET for the only significant biometric nADC-E (AUC = 0.76; *P*-value <.015) with a cutoff value of 1.63 showed a sensitivity of 68.8% and a specificity of 80%, (Figure 3; Table 7).

Univariate ROC curve analysis for MET and LGG and significant biometrics Vol-E, Vol-E/Vol-T, nADC-T, nADC-E, nCBF-T, and nCBV-T showed a significant predictive ability for these 6 biometrics. Furthermore, nCBF-T had the highest predictive capacity with a cutoff value of 4.35 AUC (0.95, *P*-value <.001), sensitivity of 93.3%, and specificity of 100%. In addition, com-

Table 6. Comparison Between LGG and MET Using Mann–Whitney *U* Test Performed for LGG and MET on Previous Statistically Significant Biometrics

	Vol-E (mL)	Vol-E/Vol T	nADC-T	nADC-E	nCBF-T	nCBV-T	nCBF-E
Mann-Whitney *U*	29.00	13.00	15.00	28.00	8.00	19.00	34.00
P-value <	0.011	0.001	0.001	0.009	0.001	0.002	0.023

Abbreviations: HGG, high-grade gliomas; LGG, low-grade gliomas; MET, metastases; nADC-T, normalized-ADC-tumor; nADC-E, normalized-ADC-edema; nCBF-T, normalized cerebral blood flow-tumor; nCBV-T, normalized cerebral blood volume-tumor; nCBF-E, nCBF-edema.
Significance after Bonferroni adjustment set at *P*-value <.016.

Table 7. ROC Analysis Performed on Biometrics for HGG, LGG, and MET

Group & Biometric	Sensitivity (%)	Specificity (%)	Cutoff Value	AUC (Area Under the Curve)	95 % CI (Confidence Interval)	P-Value
HGG/LGG						
nADC-T	85.7	80	1.76	0.87	0.73–1.00	<.003
nCBF-T	93.3	100	4.12	0.95	0.86–1.00	<.001
nCBV-T	80	90	6.06	0.91	0.79–1.00	<.001
nCBF-E	92.9	70	1.03	0.82	0.64–1.00	<.009
Combined biometrics[a]	100	100	0.50*	1.00	1.00–1.00	<.001
HGG/MET						
nADC-E	68.8	80	1.63	0.76	0.58–0.94	<.015
LGG/MET						
Vol-E (mL)	73.3	90	22.39	0.81	0.63–0.98	<.011
Vol-E/Vol-T	80	100	1.05	0.91	0.80–1.00	<.001
nADC-T	86.7	90	1.71	0.90	0.77–1.00	<.001
nADC-E	80	90	1.62	0.81	0.63–1.00	<.010
nCBF-T	93.3	100	4.35	0.95	0.84–1.00	<.001
nCBV-T	60	100	6.37	0.87	0.74–1.00	<.002
Combined biometrics[b]	93.3	100	0.60*	0.96	0.88–1.00	<.001

Abbreviations: receiver operating characteristic; HGG, high-grade gliomas; LGG, low-grade gliomas; MET, metastases; nFA-T, normalized fractional anisotropy-tumor; nADC-T, normalized-ADC-tumor; nFA-E, normalized fractional anisotropy-edema; nADC-E, normalized-ADC-edema; nCBF-T, normalized cerebral blood flow-tumor; nCBV-T, normalized cerebral blood volume-tumor; nCBF-E, nCBF-edema; nCBV-E, nCBV-edema.
Sensitivity, specificity, cutoff value, AUC, 95% confidence interval and P-value; significance level set at P-value <.05.
* Probability cutoff value generated by regression model.
[a] Combination of nADC-T, nCBF-T, nCBV-T, and nCBF-E.
[b] Combination of Vol-E, Vol-E/Vol-T, nADC-T, nADC-E, nCBF-T, and nCBV-T.

pared with nCBF-T, the biometrics Vol-E/Vol-T and nCBV-T showed equal specificity of 100%, albeit a lower AUC (0.91; P-value <.001/0.87 and <.002, respectively), and also lower sensitivity (80% and 60%, respectively) (Figure 4, A and B; Table 7).

Multivariate ROC analysis with combined significant biometrics for discrepancy between LGG and MET and biometrics Vol-E, Vol-E/Vol-T, nADC-T, nADC-E, nCBF-T, and nCBV-T (AUC = 0.96; P-value <.001) with a probability cutoff value of 0.60, generated by the logistic regression model, showed a sensitivity of 93% and a specificity of 100% (Figure 5A; Table 7).

Furthermore, HGG and LGG, with combined significant biometrics nADC-T, nCBF-T, nCBF-E, and nCBV-T, yielded an ROC curve with AUC = 1.00, P-value <.001, probability cutoff value of 0.50 for prediction probability, sensitivity of 100%, and specificity of 100% in differentiation between HGG and LGG (Figure 5B; Table 7).

The cutoff values for differentiation between HGG and LGG, HGG and MET, and LGG and MET are presented in Table 7.

DISCUSSION

In this present study, significant differences between normalized values of volumetric, perfusion, and diffusion biometrics are shown in the differentiation between LGG, HGG, and MET. Cutoff values are proposed in Table 7. The most prominent cutoff values for distinction between HGG/LGG and LGG/MET are the combined biometrics of nADC-T, nCBF-T, nCBV-T, nCBF-E with cut-off value of 0.50 for HGG/LGG as well as the
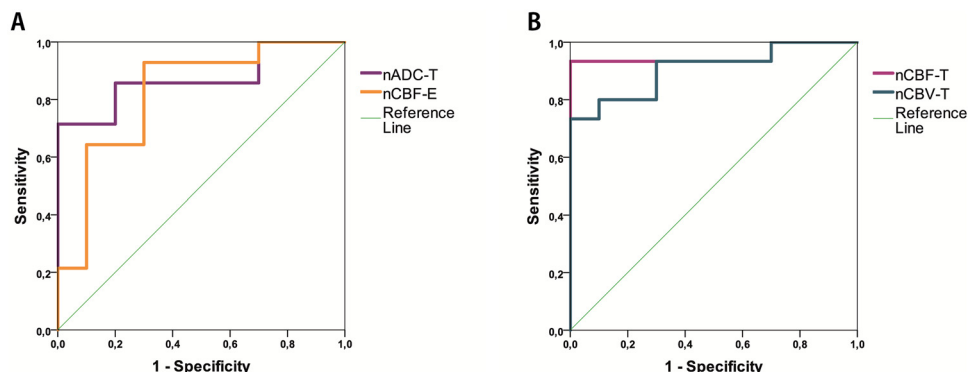

Figure 2. ROC-analysis for nADC-T and nCBF-E (A) and nCBF-T and nCBV-T (B) for distinguishing between high-grade glioma (HGG) and low-grade glioma (LGG).
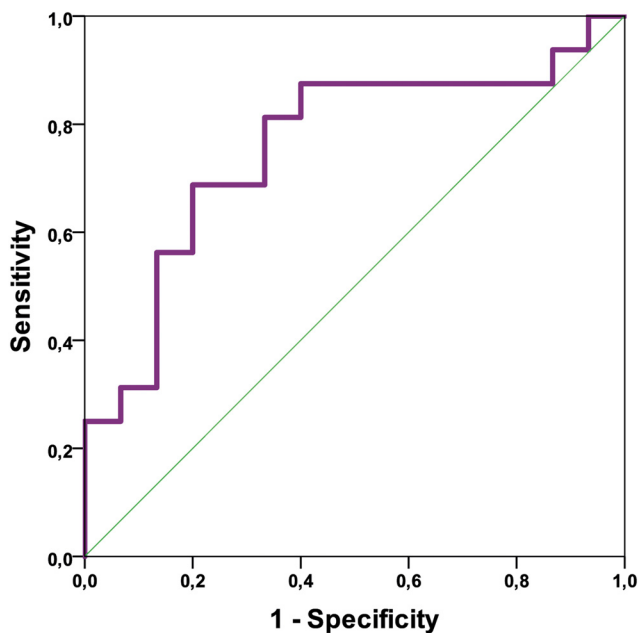
Figure 3. Receiver operating characteristic (ROC) analysis for normalized-ADC-edema (nADC-E) for distinguishing between HGG and MET

combined biometrics of Vol-E, Vol-E/Vol-T, nADC-T, nADC-E, nCBF-T, nCBV-T with cut-off value of 0.60 for LGG/MET, respectively. In addition, nCBF-T is the best single biometric, with a cutoff value of 4.12 for HGG/LGG and 4.35 for LGG/MET, resulting in a sensitivity of 93.3% and a specificity of 100% for both these groups.

The imaging characteristics of HGG and MET can be similar, as both may present with a ring enhancing partly cystic or necrotic lesion and surrounding edema (11). This can, particularly in cases of unknown primary cancer to support the diag-

nosis metastasis, be a diagnostic challenge. In addition, the differentiation between HGG and LGG cannot solely depend on the presence or absence of contrast enhancement (4). Therefore, a need exists for more accurate diagnostic tools and methods in addition to conventional MRI to improve radiological differentiation between intracranial lesions, as this may have a clinical impact in terms of treatment choice and overall prognosis for the patients (3, 12). The present multiparametric study has shown, when comparing the best single diagnostic biometric with the integrated approach, that the multiparametric approach exhibits higher sensitivity and AUC for differentiation between HGG and LGG and a higher AUC for differentiation between MET and LGG. In essence, the present study confirms the usability of volume, perfusion, and diffusion metrics for differential diagnosis in patients with primary or secondary brain tumors.

This is in accordance with some previous studies that have reported the ability of both biometrics and conventional MRI for differentiation between LGG and HGG, with some providing sensitivity and specificity for ADC, CBV, CBF, and FA (12). In addition, a previous meta-analysis study reported that the best differentiator between LGG and HGG is CBV-T (15). Our study showed that nCBF-T is the single best biometric for differentiation between LGG and HGG and between LGG and MET, whereas nADC-E, even if weak, is the sole biometric that can differentiate between HGG and MET. However, when combining imaging biometrics from both perfusion and diffusion measures such as nADC-T, nCBF-T, nCBV-T, and nCBF-E, a sensitivity and specificity of 100% can be achieved in distinguishing HGG from LGG.

Our findings of lower nCBV and nCBF in LGG compared with those in HGG are in accordance with previous studies (19, 26). The present study's ROC analysis when combining, in our case, nADC-T, nCBF-T, nCBF-E and nCBV-T, yields an ROC curve with AUC = 1.00 (P-value <.001) with a sensitivity and specificity of 100% to differentiate between HGG and LGG. This is well in accordance with the accuracy for the combination of nCBF-T and nCBV-T, with a sensitivity of 100% and a specificity
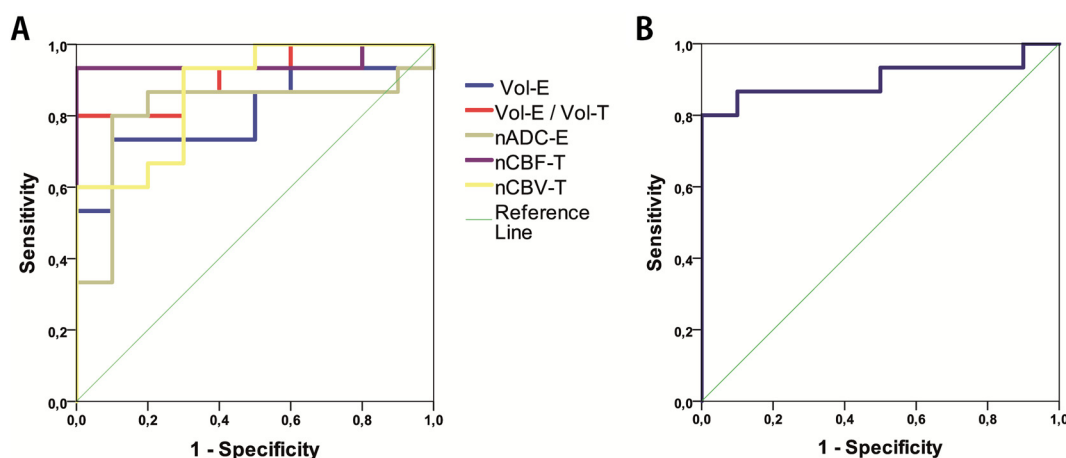

Figure 4. ROC analysis for Vol-E, Vol-E/Vol-T, nADC-E, nCBF-T, and nCBV-T (A) and nADC-T for distinguishing between LGG and MET (B).
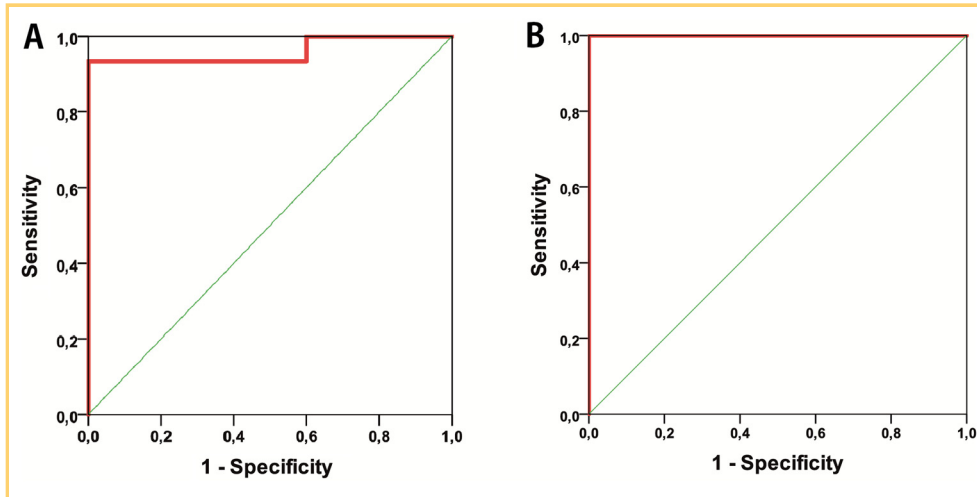
Figure 5. ROC-analysis for combined biometrics (A–B); Vol-E, Vol-E/Vol-T, nADC-T, nADC-E, nCBF-T and nCBV-T for distinguishing between LGG and MET (A) and nADC-T, nCBF-T, nCBV-T and nCBF-E for distinguishing between HGG and LGG (B).

of 90.9% and AUC = 0.992, reported in a previous study (19), as well as other studies that have shown that nCBF and nCBV have the highest specificity and sensitivity in differentiating between LGG and HGG (27–29).

A significant difference within edematous tissue between HGG and LGG was the presence of only reduced nCBF values in the peritumoral edematous tissue in the LGG compared with that in the HGG. A possible explanation for the differences may be that perfusion may be reduced owing to an increase in the local pressure exerted upon vasculature because of fluid leakage into an enclosed space as suggested by some authors (30, 31). HGG showed the highest median Vol-T (40.25 mL), the lowest Vol-E (26.58 mL), and the highest nCBF-T (7.91). Intratumoral compressive growth-induced stress results not only in the formation of necrosis within the tumor interior but also deforms and compresses vessels. Defect tumor vessels owing to angiogenesis result in hyperpermeability and increased fluid flux into the interstitium that raises interstitial fluid pressure and consequently reduces perfusion, as the difference in microvascular pressure in upstream and downstream segments of the vasculature reduces (32). This may also explain why HGG in this cohort exhibits the lowest perilesional edema tissue perfusion (nCBF-E) of 0.59.

In the present study, combining VOL-E, VOL-E/VOL-T, nADC-T, nADC-E, nCBF-T, nCBV-T yielded a sensitivity of 93.3% but still 100% specificity for distinguishing LGG from MET. Even though nCBF-T also reached the same level of accuracy with regards to sensitivity and specificity, the combined approach had higher AUC, suggesting that the combined approach is more plausible to use.

Although perfusion metrics such as nCBV and nCBF in both tumor and edema could differentiate between HGG and LGG, only nADC in the tumor (nADC-T) could distinguish HGG from LGG and LGG from MET. Cellular density is correlated with the pathological grades of glioma, that is, glioma with a higher cell density has lower ADC values than gliomas with a lower cell density (33). This may explain our finding of significantly higher nADC-T in LGG compared with that in HGG and MET. As we excluded cystic, hemorrhagic, or necrotic parts in our measurement, we can speculate that higher nADC values imply less density of cells in selected volumes of tissue in LGG and higher cell density in the HGG, reflecting the lower nADC-T in HGG

when compared with LGG. Also, the similar median values of nADC-T for MET and HGG imply that these 2 groups have a similar cellular density in the central parts of the tumor. However, the median nADC-E being higher in MET than in HGG can be explained by MET having few pathological cellular components in the surrounding perilesional edema tissue secondary to higher tissue displacement and increased water content (34). In addition, it has been shown that MET had higher ADC in perienhancing regions than HGG, suggestive of higher fluid production/extravasation (30). At the same time, there is also the possibility that the higher ADC in MET is because a more rapid fluid expansion per time unit than HGG and LGG in the early phases of tumor manifestation in the brain; this is further supported by MET also having the largest Vol-E (50.28 mL) and the largest Vol-E/Vol-T ratio (2.88) of the 3 groups. Our findings of highest diffusion in the perilesional edema of MET compared with HGG is in accordance with the findings of a previous study (35).

Contradictory to the present and most previous studies (35, 36), significant differences between maximum intratumor FA values between LGG and HGG have been reported in 1 study (37). However, the result from that study might be questionable, as the authors did not correlate their maximum FA values with maximum FA values for normal tissue, and thus, they did not adjust for intraindividual variations. In the present study, comparison was made with normalized values to give the best inter- and intraobserver reproducibility as reported previously (20–22). Minor differences between our study and previous studies in terms of specificity may be because of inconsistencies in the sample size or methodology, in which some studies chose not to normalize biometrics with contralateral normal-appearing tissue. This may have implications, as some biometrics that are not significantly differing between groups may be reported as such owing to intraindividual differences.

There are some incongruences in the literature with regard to differentiation between MET and HGG by means of nCBV-T and nADC-T, as some previous studies have shown difficulties in differentiating HGG from MET using quantitative biometrics such as nCBV-T (30, 38), and other studies have shown that normalized CBV in perilesional edema can help differentiate MET from HGG with 90% sensitivity and 100% specificity (29).

Furthermore, several other studies have shown higher ADC-values in perilesional edema of MET compared with the corresponding tissue in HGG; however, these studies did not provide sensitivity, specificity, or cutoff values for the distinction between tumor types (30, 39). Particularly surprising were the findings in a larger cohort of patients with MET, which showed that nADC-T and n-CBV-T values do not differ between histologically different MET (40). Furthermore, a meta-study concludes that MET cannot be differentiated reliably from HGG on the basis of ADC and CBV (15). This present study found that only nADC-E could distinguish HGG from MET.

In contrast to the difficulties in differentiating HGG from MET, several biometrics investigated here differentiated LGG from MET. Vol-E, Vol-E/Vol-T, nADC-T, and nADC-E, as well as nCBF-T and nCBV-T, can all be used for differential diagnosis between LGG and MET. Findings, which are supported by some previous studies, showed significantly lower nCBV in LGG compared with MET and HGG and higher minimum ADC levels in LGG compared with MET (15, 41).

Finally, it is acknowledged that the present study has some limitations such as the relatively small group sizes; even though the size is adequate for performing the statistical evaluations, one should not exclude the possibility that sampling errors may occur or that tumors have nonlinear behavior or growth. At the time of this study, IDH was not assessed in all patients with glioblastoma. IDH mutations are, therefore, not included as a confounder in the analysis. Histopathological diagnosis of the tumors was presumed to be 100% correct.

We have not correlated our measurements with the results of a possible treatment with steroids, a drug that may have some effect on the perfusion metrics and reduce the perilesional edema.

In addition, the probabilities generated by the logistic regression model used for the ROC analysis, the chosen method, that is, machine learning algorithm, cannot generate further cutoff values, that is, the exact cutoff values in each biometric in the combined analysis, than is already provided via the ROC analysis, that is, probability values (Table 7).

There may be further value in the proposed model for predictions on the prognosis of OS and MTP; albeit this being out of the scope of this study, it is reasonable to externally validate the model on a larger cohort of patients and conduct follow-ups with regard to OS and MTP.

CONCLUSION

The present study clearly shows and confirms the advantages of an integrative approach by measuring the volume, perfusion, and diffusion metrics. Such an integrated approach can, as presented in this study, yield cutoff values and improve sensitivity and specificity while aiding the clinician in preoperative differentiation between LGG, HGG, and MET. Furthermore, this study adds to the growing body of evidence in a clinical field in need of validation and standardization.

REFERENCES

1. Chen L, Zou X, Wang Y, Mao Y, Zhou L. Central nervous system tumors: a single center pathology review of 34,140 cases over 60 years. BMC Clin Pathol. 2013; 13:14.
2. Louis DN, Perry A, Reifenberger G, von Deimling A, Figarella-Branger D, Cavenee WK, Ohgaki H, Wiestler OD, Kleihues P, Ellison DW. The 2016 World Health Organization classification of tumors of the central Nervous System: a summary. Acta Neuropathol. 2016;131:803–820.
3. Bush NA, Chang SM, Berger MS. Current and future strategies for treatment of glioma. Neurosurg Rev. 2017;40:1–14.
4. Scott JN, Brasher PMA, Sevick RJ, Rewcastle NB, Forsyth PA. How often are nonenhancing supratentorial gliomas malignant? A population study. Neurology. 2002 24;59:947–949.
5. Brasil Caseiras G, Ciccarelli O, Altmann DR, Benton CE, Tozer DJ, Tofts PS, Yousry TA, Rees J, Waldman AD, Jäger HR. Low-grade gliomas: six-month tumor growth predicts patient outcome better than admission tumor volume, relative cerebral blood volume, and apparent diffusion coefficient. Radiology. 2009;253: 505–512.
6. Piroth MD, Holy R, Pinkawa M, Stoffels G, Kaiser HJ, Galldiks N, Herzog H, Coenen HH, Eble MJ, Langen KJ. Prognostic impact of postoperative, pre-irradiation (18)F-fluoroethyl-l-tyrosine uptake in glioblastoma patients treated with radiochemotherapy. Radiother Oncol. 2011;99:218–224.
7. Lacroix M, Abi-Said D, Fourney DR, Gokaslan ZL, Shi W, DeMonte F, Lang FF, McCutcheon IE, Hassenbusch SJ, Holland E, Hess K, Michael C, Miller D, Sawaya R.. A multivariate analysis of 416 patients with glioblastoma multiforme: prognosis, extent of resection, and survival. J Neurosurg. 2001;95:190–198.
8. McGirt MJ, Chaichana KL, Gathinji M, Attenello FJ, Than K, Olivi A, Weingart JD, Brem H, Quiñones-Hinojosa AR. Independent association of extent of resection with survival in patients with malignant brain astrocytoma. J Neurosurg. 2009;110:156–162.
9. Sanai N, Polley M-Y, McDermott MW, Parsa AT, Berger MS. An extent of resection threshold for newly diagnosed glioblastomas. J Neurosurg. 2011;115:3–8.
10. Pignatti F, van den Bent M, Curran D, Debruyne C, Sylvester R, Therasse P, Afra D, Cornu P, Bolla M, Vecht C, Karim AB; European Organization for Research and Treatment of Cancer Brain Tumor Cooperative Group; European Organization for Research and Treatment of Cancer Radiotherapy Cooperative Group. Prognostic factors for survival in adult patients with cerebral low-grade glioma. J Clin Oncol. 2002;20:2076–2084.
11. Gavrilovic IT, Posner JB. Brain metastases: epidemiology and pathophysiology. J Neurooncol. 2005;75:5–14.
12. Fouke SJ, Benzinger T, Gibson D, Ryken TC, Kalkanis SN, Olson JJ. The role of imaging in the management of adults with diffuse low grade glioma: A systematic review and evidence-based clinical practice guideline. J Neurooncol. 2015; 125:457–479.
13. Svolos P, Kousi E, Kapsalaki E, Theodorou K, Fezoulidis I, Kappas C, Kappas C, Tsougos I. The role of diffusion and perfusion weighted imaging in the differential diagnosis of cerebral tumors: a review and future perspectives. Cancer Imaging. 2014;14:20.
14. Zhou C, Yang Z, Yao Z, Yin B, Pan J, Yu Y, Zhu W, Hua W, Mao Y. Segmentation of peritumoral oedema offers a valuable radiological feature of cerebral metastasis. Br J Radiol. 2016;89:20151054.
15. Usinskiene J, Ulyte A, Bjørnerud A, Venius J, Katsaros VK, Rynkeviciene R, Letautiene S, Norkus D, Suziedelis K, Rocka S, Usinskas A, Aleknavicius E. Optimal differentiation of high- and low-grade glioma and metastasis: a meta-analysis of perfusion, diffusion, and spectroscopy metrics. Neuroradiology. 2016;58:339–350.
16. Steyerberg EW, Vickers AJ, Cook NR, Gerds T, Gonen M, Obuchowski N, Pencina MJ, Kattan MW. Assessing the performance of prediction models: a framework for traditional and novel measures. Epidemiology. 2010;21:128–138.

17. Jung SC, Choi SH, Yeom JA, Kim J-H, Ryoo I, Kim SC, Shin H, Lee AL, Yun TJ, Park CK, Sohn CH, Park SH. Cerebral blood volume analysis in glioblastomas using dynamic susceptibility contrast-enhanced perfusion MRI: a comparison of manual and semiautomatic segmentation methods. PLoS One. 2013;8: e69323.

18. Bennett IJ, Madden DJ, Vaidya CJ, Howard D V, Howard JH Jr. Age-related differences in multiple measures of white matter integrity: A diffusion tensor imaging study of healthy aging. Hum Brain Mapp. 2010;31:378–390.

19. Hakyemez B, Erdogan C, Ercan I, Ergin N, Uysal S, Atahan S. High-grade and low-grade gliomas: differentiation by using perfusion MR imaging. Clin Radiol. 2005;60:493–502.

20. Caseiras GB, Chheang S, Babb J, Rees JH, Pecerrelli N, Tozer DJ, Benton C, Zagzag D, Johnson G, Waldman AD, Jäger HR, Law M. Relative cerebral blood volume measurements of low-grade gliomas predict patient outcome in a multi-institution setting. Eur J Radiol. 2010 Feb;73:215–220.

21. Wetzel SG, Cha S, Johnson G, Lee P, Law M, Kasow DL, Pierce SD, Xue X. Relative cerebral blood volume measurements in intracranial mass lesions: interobserver and intraobserver reproducibility study. Radiology. 2002;224:797–803.

22. Law M, Yang S, Wang H, Babb JS, Johnson G, Cha S, Knopp EA, Zagzag D. Glioma grading: sensitivity, specificity, and predictive values of perfusion MR imaging and proton MR spectroscopic imaging compared with conventional MR imaging. AJNR Am J Neuroradiol. 2003;24:1989–1998.

23. Knutsson L, Ståhlberg F, Wirestam R. Absolute quantification of perfusion using dynamic susceptibility contrast MRI: pitfalls and possibilities. MAGMA. 2010;23: 1–21.

24. Holm S. A simple sequentially rejective multiple test procedure. Scand J Stat. 1979 6:65–70.

25. Halligan S, Altman DG, Mallett S. Disadvantages of using the area under the receiver operating characteristic curve to assess imaging tests: A discussion and proposal for an alternative approach. Eur Radiol. 2015;25:932–939.

26. Morita N, Wang S, Chawla S, Poptani H, Melhem ER. Dynamic susceptibility contrast perfusion weighted imaging in grading of nonenhancing astrocytomas. J Magn Reson Imaging. 2010;32:803–808.

27. Smitha KA, Gupta AK, Jayasree RS. Relative percentage signal intensity recovery of perfusion metrics—an efficient tool for differentiating grades of glioma. Br J Radiol. 2015;88:20140784.

28. Bauer AH, Erly W, Moser FG, Maya M, Nael K. Differentiation of solitary brain metastasis from glioblastoma multiforme: a predictive multiparametric approach using combined MR diffusion and perfusion. Neuroradiology. 2015;57:697–703.

29. Sparacia G, Gadde JA, Iaia A, Sparacia B, Midiri M. Usefulness of quantitative peritumoural perfusion and proton spectroscopic magnetic resonance imaging evaluation in differentiating brain gliomas from solitary brain metastases. Neuroradiol J. 2016;29:160–167.

30. Chiang IC, Kuo YT, Lu CY, Yeung KW, Lin WC, Sheu FO, Liu GC. Distinction between high-grade gliomas and solitary metastases using peritumoral 3-T magnetic resonance spectroscopy, diffusion, and perfusion imagings. Neuroradiology. 2004;46:619–627.

31. Hossman KA, Blöink M. Blood flow and regulation of blood flow in experimental peritumoral edema. Stroke. 1981;12:211–217.

32. Jain RK, Martin JD, Stylianopoulos T. The role of mechanical forces in tumor growth and therapy. Annu Rev Biomed Eng. 2014;16:321–346.

33. Chen SD, Hou PF, Lou L, Jin X, Wang TH, Xu JL. The correlation between MR diffusion-weighted imaging and pathological grades on glioma. Eur Rev Med Pharmacol Sci. 2014;18:1904–1909.

34. Guzman R, Altrichter S, El-Koussy M, Gralla J, Weis J, Barth A, Seiler RW, Schroth G, Lövblad KO. Contribution of the apparent diffusion coefficient in perilesional edema for the assessment of brain tumors. J Neuroradiol. 2008;35: 224–229.

35. Lu S, Ahn D, Johnson G, Cha S. Peritumoral diffusion tensor imaging of high-grade gliomas and metastatic brain tumors. AJNR Am J Neuroradiol. 2003;24: 937–941.

36. Ryu YJ, Choi SH, Park SJ, Yun TJ, Kim JH, Sohn CH. Glioma: application of whole-tumor texture analysis of diffusion-weighted imaging for the evaluation of tumor heterogeneity. PLoS One. 2014;9:e108335.

37. Jolapara M, Patro SN, Kesavadas C, Saini J, Thomas B, Gupta AK, Bodhey N, Radhakrishnan VV. Can diffusion tensor metrics help in preoperative grading of diffusely infiltrating astrocytomas? A retrospective study of 36 cases. Neuroradiology. 2011;53:63–68.

38. Law M, Cha S, Knopp EA, Johnson G, Arnett J, Litt AW. High-grade gliomas and solitary metastases: differentiation by using perfusion and proton spectroscopic MR imaging. Radiology. 2002;222:715–721.

39. Pavlisa G, Rados M, Pavlisa G, Pavic L, Potocki K, Mayer D. The differences of water diffusion between brain tissue infiltrated by tumor and peritumoral vasogenic edema. Clin Imaging. 2009;33:96–101.

40. Gaudino S, Di Lella GM, Russo R, Lo Russo VS, Piludu F, Quaglio FR, Gualano MR, De Waure C, Colosimo C. Magnetic resonance imaging of solitary brain metastases: main findings of nonmorphological sequences. Radiol Med. 2012; 117:1225–1241.

41. Kitis O, Altay H, Calli C, Yunten N, Akalin T, Yurtseven T. Minimum apparent diffusion coefficients in the evaluation of brain tumors. Eur J Radiol. 2005;55: 393–400.